Supporting Information -- Minimal Molecular Building Blocks for Screening in Quasi-Two-Dimensional Organic–Inorganic Lead-Halide Perovskites

*Jack McArthur[1,2], Marina R. Filip[3], Diana Y. Qiu[1,4]**

1. Department of Physics, Yale University, New Haven, Connecticut 06520, USA

2. Department of Physics, University of California at Berkeley, California 94720, USA

3. Department of Physics, University of Oxford, Clarendon Laboratory, Oxford OX1 3PU, United Kingdom

4. Department of Mechanical Engineering and Materials Science, Yale University, New Haven, Connecticut 06520, USA

KEYWORDS. Layered perovskites, excited states, screening, optical properties, ab initio

Outline:

1. Computational Setup
2. Single-molecule justification

3. Density Functional Theory Calculations
4. *GW*-BSE Calculations
    a. Band convergence

Computational Setup

For all calculations, we make use of the smallest n=1 RP perovskite unit cells with undistorted octahedra as model structures. We use the same structures defined in Ref. [1], a set of structures built from undistorted $PbBr_4$ octahedral layers with the same 2.94 Å Pb-Br bond lengths as the cubic perovskite $CsPbBr_3$ and interlayer distances determined from experiments. Each of the model calculation unit cells contains two $PbBr_4$ subunits and four organic cation molecules; as such, we specify that four electrons per unit cell are transferred from cationic to anionic sublattices when performing mean field calculations for the IPSA-2C method. The structures of all four perovskites as well as their Cs-substituted analogs can be seen in Figure S1. We justify this assumption on the basis of Bader Charge Analysis in Table S1, as implemented in the Quantum Espresso software package.[2, 3] To construct Cs-substituted unit cells, we replace the molecular cations with Cs atoms, then relax the positions of the Cs atoms while keeping the $PbBr_4$ layers and lattice parameters fixed.

When using the IPSA-2C method, we compensate for the formal charges of the EA and BA perovskite cations/anions using a jellium background; however, for the largest two perovskites, PMA and NMA, (with large volumes of vacuum in the single-sublattice unit cells), the jellium model can give rise to unphysical valence states for the $PbBr_4$ calculation within the positively-charged vacuum regions, so instead, we perform calculations on neutrally charged organic and inorganic subsystems for these species and then adjusted the band occupations to those dictated by formal charges. The jellium background method performs better for the EA and BA species

(those for which it can be used at all), as the transferred electrons' contributions to $v_{Hartree}$ or v_{xc} in the Kohn-Sham equations are more significant in smaller systems; comparisons of bandstructures and band gaps produced by both methods can be found in Fig. S2 and Table S2. We recommend employing the jellium model when the anionic subsystem calculation contains no regions of vacuum with a total homogeneous background charge density greater than +¿e∨¿ to avoid spurious states, and recommend testing both methods. For systems with molecular substructures that occupy large volumes, the occupation-adjustment method performs exceedingly well (<0.9% error in band gaps) as organic/inorganic wavefunction hybridization is less significant, especially in the case when the organic molecules contain large conjugated molecular orbitals.

Single-molecule justification

To justify the single-molecule treatment of the dielectric screening, we assume that the polarizability of one molecular cation in our model structures differs minimally from the polarizability of an isolated molecular cation. In Fig. S3 we show the DFT bandstructures of the four NMA molecular cations sharing one unit cell (as used in the IPSA-2C calculations with results seen in Figs. 1-4) vs. only a single NMA molecule in the same unit cell. The energy level splitting in the four-molecule calculation is on the order of 10 meV, suggesting only small wavefunction overlap between the molecules. Somewhat larger errors are seen only in the splitting of the NMA cation LUMO. The constant energy shift between the two bandstructures is due to the increased Coulombic repulsion in the four-molecule system, though this does not affect the calculation of polarizability. We also argue in the text that band edge features are well-mimicked by the Cs-substitution method because the band edge generally has the character of the

inorganic lattice. The GW quasiparticle bandstructure of $(NMA)_2PbBr_4$ with the k-resolved, DFT-derived density of states projected onto the organic/inorganic sublattices is shown in Fig. S4.

To justify further the separability of the molecules, we calculate DFT wavefunctions on each of two adjacent NMA molecules, A and B, at their adjacent positions within the $(NMA)_2PbBr_4$ unit cell, and calculated the total inner product of all single-particle states between the molecules, that is, $\sum_{i,j=occ} \left\langle \psi_i^A \middle| \psi_j^B \right\rangle$. The two molecules in these positions are separated by a minimum distance of 3.6 $\mathring{A}$, and the resulting overlap is found to be 1.55 electrons. With 60 valence electrons considered in our calculation per molecule, the expected wavefunction overlap of a valence electron with the adjacent NMA molecules is 2.6% (all NMA molecules laterally adjacent to a molecule A are equivalent to molecule B; see Figure S1) and naturally lower for other pairings of molecules.

Density functional theory calculations

All mean field calculations are performed within the Perdew-Burke-Erzerhof parametrization of the generalized gradient approximation (PBE)[4] via the Quantum Espresso code.[2, 3] For all calculations we use the standard optimized norm-conserving Vanderbilt pseudopotentials,[5, 6] a plane wave cutoff of 50 Ry, and a $6 \times 2 \times 6$ k-grid size. The valence configurations considered are: Pb $6s^2 5d^{10} 6p^2$, Br $4s^2 4p^5$, N $2s^2 2p^3$, C $2s^2 2p^2$, H $1s^1$, Cs $5s^2 5p^6 6s^1$. All calculations fully take into account spin-orbit coupling.

***GW*+BSE calculations**

All excited state calculations are performed within the *GW* approximation and the Bethe-Salpeter equation, as implemented in the BerkeleyGW code.[7-9] Dielectric matrix calculations for all systems were carried out using the Godby-Needs plasmon pole model to approximate the frequency-dependent dielectric function.[10] We used a $6 \times 2 \times 6$ q-point grid half-shifted in the in-plane direction and a 6 Ry energy cutoff. The numbers of empty bands considered for the full calculations varies from 564-682 as shown in Table S3, a setup which improves upon the convergence with respect to empty states shown in Ref [1], where the computed quasiparticle band gap was converged within 0.1-0.2 eV. QP band gaps thus computed differ from those reported in Ref [1] by less than 0.1 eV.

Bandstructure plots for all four perovskites are shown in Figure S5. DFT@PBE electronic band structures calculated for the Cs-substituted band structures show a four-fold-degenerate conduction band bottom and valence band top. In the bandstructures shown in Fig. S5, there is a 10-150 meV splitting of both sets of degenerate bands due to the presence of the organic molecules. In Ref. [1], this degeneracy breaking is not seen in electronic structure calculations using experimental structures of these species (including octahedral tilting), suggesting they are artefacts of our choice of model structures. As such, when calculating quasiparticle band gaps of each species, as plotted in Figs. 1c and 1d and as used to obtain exciton binding energies in the text, we calculate the energy difference between the average of the four lowest conduction bands and the average of the four highest valence bands.

Band convergence

To ensure similar levels of convergence between our full calculations and IPSA-2C calculations, we develop a scheme to conserve the same number of empty bands in both methods: in the

IPSA-2C method, the number of empty bands used in each full calculation are divided between the separate IPSA-2C dielectric matrix calculations for the anions and cations. The exact number of empty bands N_{PbBr_4} and N_{RNH_3} are chosen to be proportional to the number of filled bands in the anion and cation subsystems. A smaller number of bands is used for the Cs-substituted model structures, chosen to be proportional to the smaller number of filled bands relative to the full structures. In Fig. S6, we show convergence of the head of the inverse dielectric matrix for a given **q**-point, $\varepsilon^{-1}\left(G=G'=0, q=\frac{1}{6}\hat{x}\right)$, for the calculations of cells containing a single NMA molecule and four NMA molecules as two example subsystems. In this case, dividing the number of occupied and unoccupied bands by four actually brings us closer to the single-molecule infinitely converged result (1.26% error) than we were originally to the four-molecule infinitely converged result (2.60% error); our guideline of dividing the number of bands evenly across subsystems ensures that our results are accurate up to limitations of polarizability separation rather than limitations of our band convergence scheme.

Quasiparticle energies are computed within the single-shot G_0W_0 approximation with the static remainder approximation[8] to facilitate convergence with respect to empty electronic states. We calculate quasiparticle energies with a 6 Ry cutoff and a Γ-centered grid of $6\times2\times6$ k-points. Optical absorption spectra are calculated using the Bethe-Salpeter equation as implemented in the BerkeleyGW code.[11] We calculate the electron-hole interaction kernel on a $6\times2\times6$ Γ-centered coarse grid with eight valence and conduction bands, then interpolate this kernel onto a fine grid of size $24\times1\times24$. For the calculation of optical absorption spectra, we make use of a $24\times1\times24$ fine k-point grid, using momentum matrix elements rather than velocity matrix elements for reduced computational cost. Exciton binding energies thus computed differ from

those reported in Ref. [1] by up to 100 meV, and we assign this difference primarily to the improved convergence of the static dielectric constant with respect to the number of empty states. Overall trends in the computation of exciton binding energies for these model structures are the same as those reported in Ref. [1].

Benchmarking for ε^{-1} calculations as seen in Fig. 4c was performed using the epsilon.cplx.x code in (CPU-based) version 3.0 of the BerkeleyGW package on the TACC Frontera cluster. The total node-hours to calculate the dielectric matrix ε^{-1} was extrapolated from the total CPU time to calculate ε^{-1} for one of the 72 q-points, minus the reported I/O time, on a configuration of 72 nodes, using one MPI task per node and 56 OpenMP threads per task.

FIGURES.

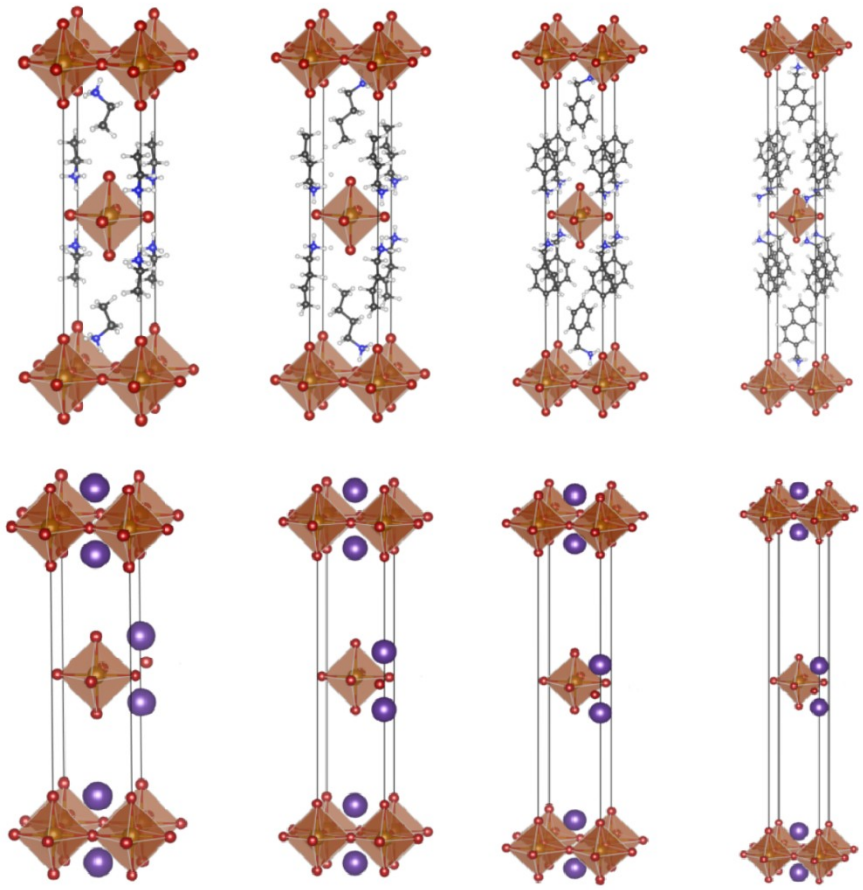

Figure S1. Unit cells of the four perovskites studied and their Cs-substituted analogs: from left to right, $(EA)_2PbBr_4$ and $Cs^{EA}{}_2PbBr_4$, $(BA)_2PbBr_4$ and $Cs^{BA}{}_2PbBr_4$, $(PMA)_2PbBr_4$ and $Cs^{PMA}{}_2PbBr_4$, and $(NMA)_2PbBr_4$ and $Cs^{NMA}{}_2PbBr_4$.

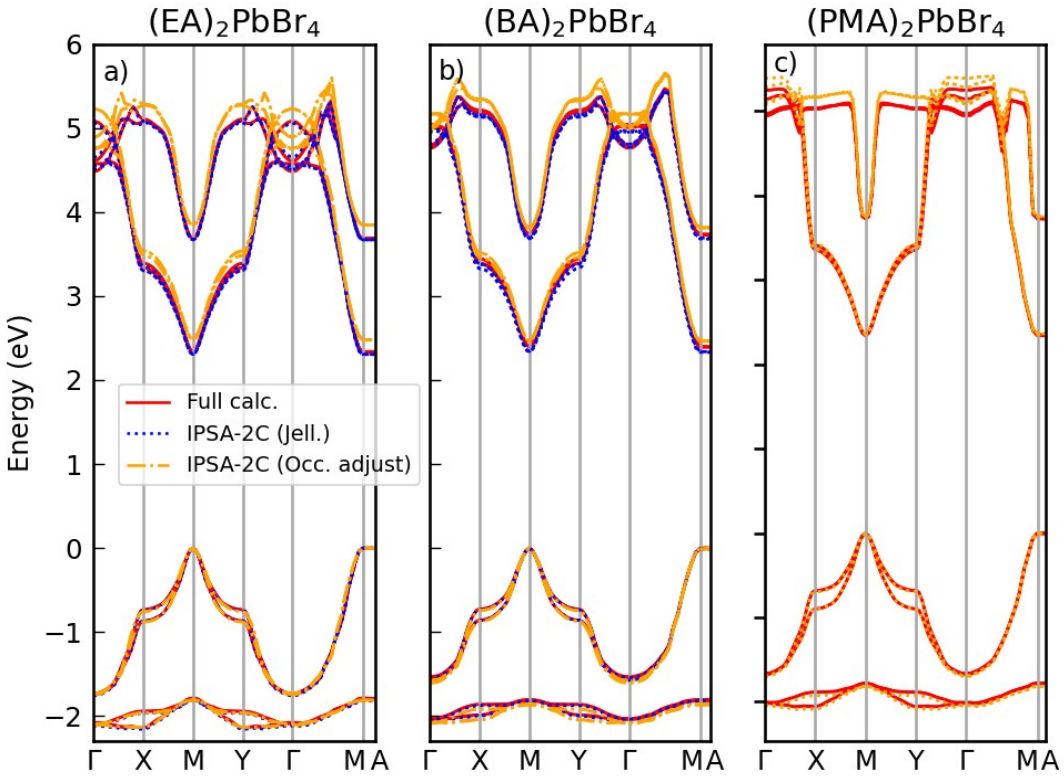

Figure S2. Comparison of the jellium-based and occupation-adjustment-based methods for IPSA-2C cation/anion separation in $(EA)_2PbBr_4$ and $(BA)_2PbBr_4$ with occupation-adjustment-based IPSA-2C for $(PMA)_2PbBr_4$ as a reference.

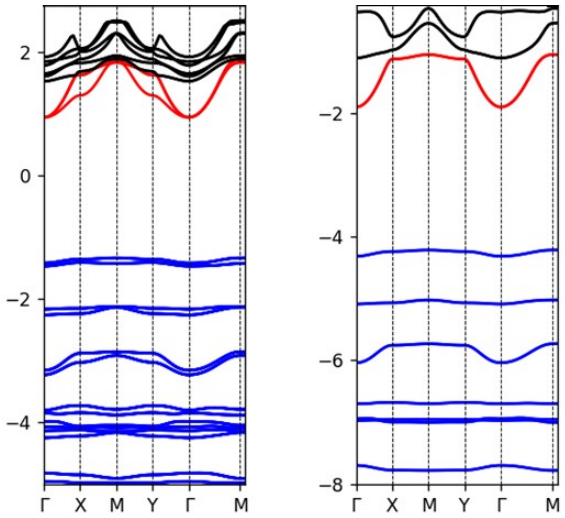

Figure S3. Band structures of 4 NMA molecules in one perovskite unit cell (left) vs. 1 NMA molecule (right). Blue bands are filled, red bands are filled in the uncharged NMA state and empty in the NMA^+ state, and black bands are unfilled.

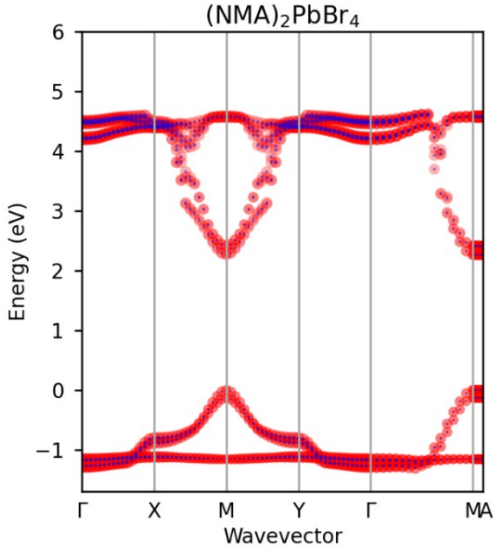

Figure S4. G_0W_0 quasiparticle bandstructure of $(NMA)_2PbBr_4$, colored by the DFT density of states projected onto Pb and Br atoms (red) and C and N atoms (blue).

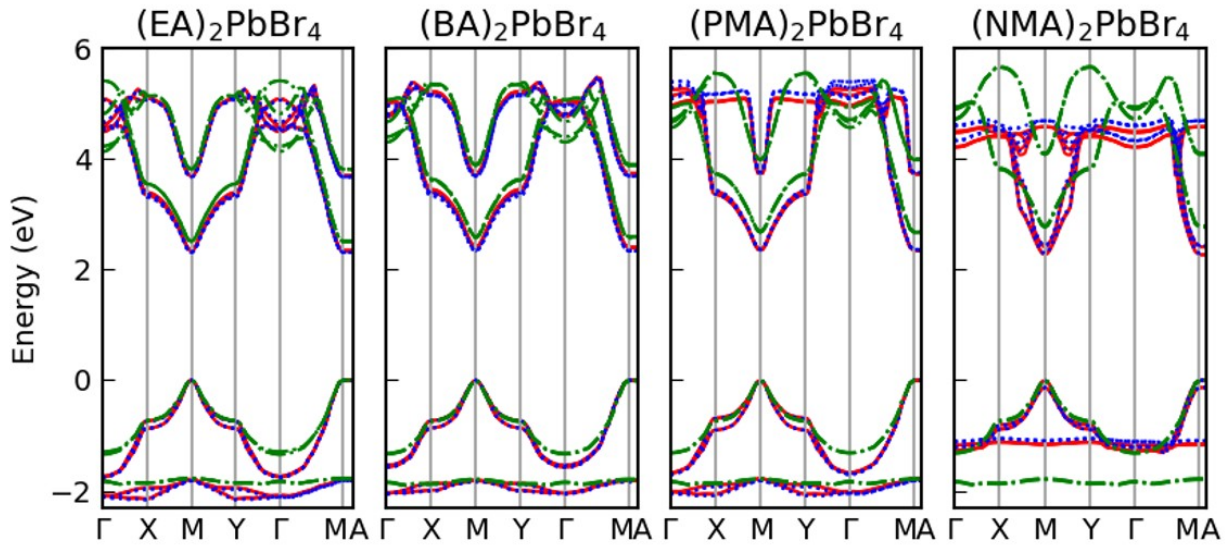

Figure S5. G_0W_0 quasiparticle bandstructure of all four perovskite structures organized by increasing cation size/interlayer distance, obtained by direct calculation (red solid line), in the IPSA-2C method (blue dotted line), and with Cs^A cation substitution (green dashed line).

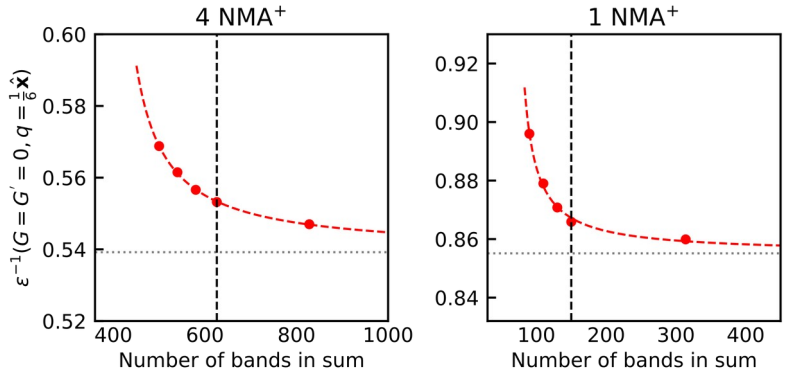

Figure S6. Convergence with respect to total number of bands of $\varepsilon^{-1}\left(G=G'=0, q=\frac{1}{6}\hat{x}\right)$ calculated for an $(NMA)_2PbBr_4$ unit cell containing four NMA molecules (left) and a single NMA molecule (right). The number of bands used in our calculations are indicated by the black dashed lines, and the fitted infinitely converged results are indicated by the grey dotted lines.

TABLES.

Material	Excess charge per molecule
$(EA)_2PbBr_4$	+0.788*e*
$(BA)_2PbBr_4$	+0.778*e*
$(PMA)_2PbBr_4$	+0.770*e*
$(NMA)_2PbBr_4$	+0.769*e*

Table S1. Excess positive charge per organic molecule in each model structure, as determined via Bader Charge Analysis.

	Full calc.	IPSA-2C (jellium)	IPSA-2C (occ. adjustment)
$(EA)_2PbBr_4$	2.339 eV	2.306 eV (-1.4%)	2.482 eV (+6.1%)
$(BA)_2PbBr_4$	2.399 eV	2.338 eV (-2.5%)	2.467 eV (+2.8%)
$(PMA)_2PbBr_4$	2.347 eV	-	2.359 eV (+0.5%)
$(NMA)_2PbBr_4$	2.401 eV	-	2.422 eV (+0.9%)

Table S2. Comparison of band gaps by jellium-based and occupation-adjustment-based methods for IPSA-2C cation/anion separation.

Perovskite	Filled bands	Cell volume, ($a.u.^3$)	Total bands, direct calc.	$PbBr_4$ bands (V + C),	Cation bands (V + C),

				IPSA-2C	IPSA-2C
$(Cs^A)_2PbBr_4$	120	-	684	-	-
$(EA)_2PbBr_4$	168	5474.1	732	88 + 294	80 + 268
$(BA)_2PbBr_4$	216	6440.4	812	88 + 298	128 + 298
$(PMA)_2PbBr_4$	256	7766.0	890	88 + 316	168 + 316
$(NMA)_2PbBr_4$	336	9623.7	1018	88 + 342	248 + 342

Table S3. Numbers of bands used in the polarizability calculations of the four perovskite structures in full calculations and IPSA-2C calculations.

REFERENCES

1. Filip, M. R.; Qiu, D. Y.; Del Ben, M.; Neaton, J. B. *Nano Letters* **2022,** 22, (12), 4870-4878.
2. Giannozzi, P.; Andreussi, O.; Brumme, T.; Bunau, O.; Nardelli, M. B.; Calandra, M.; Car, R.; Cavazzoni, C.; Ceresoli, D.; Cococcioni, M. *Journal of physics: Condensed matter* **2017,** 29, (46), 465901.
3. Giannozzi, P.; Baroni, S.; Bonini, N.; Calandra, M.; Car, R.; Cavazzoni, C.; Ceresoli, D.; Chiarotti, G. L.; Cococcioni, M.; Dabo, I. *Journal of physics: Condensed matter* **2009,** 21, (39), 395502.
4. Perdew, J. P.; Burke, K.; Ernzerhof, M. *Physical Review Letters* **1996,** 77, (18), 3865-3868.
5. Hamann, D. *Physical Review B* **2013,** 88, (8), 085117.
6. van Setten, M. J.; Giantomassi, M.; Bousquet, E.; Verstraete, M. J.; Hamann, D. R.; Gonze, X.; Rignanese, G.-M. *Computer Physics Communications* **2018,** 226, 39-54.
7. Barker, B. A.; Deslippe, J.; Lischner, J.; Jain, M.; Yazyev, O. V.; Strubbe, D. A.; Louie, S. G. *Physical Review B* **2022,** 106, (11), 115127.
8. Deslippe, J.; Samsonidze, G.; Strubbe, D. A.; Jain, M.; Cohen, M. L.; Louie, S. G. *Computer Physics Communications* **2012,** 183, (6), 1269-1289.
9. Hybertsen, M. S.; Louie, S. G. *Physical Review B* **1986,** 34, (8), 5390-5413.
10. Godby, R. W.; Needs, R. J. *Physical Review Letters* **1989,** 62, (10), 1169-1172.
11. Rohlfing, M.; Louie, S. G. *Physical Review B* **2000,** 62, (8), 4927-4944.